Extenuating Chatter Vibration in Milling Process Using a New Ensemble Approach

Rohit Mishra[1] · **Bhagat Singh**[1]

Abstract

Background Milling process contributes 60–70% of the finishing process in machining industries. Surface finish of the product is greatly influenced by the nature of chatter vibration initiated during milling due to its self-generating chatter phenomenon.

Purpose To ascertain the stability regimes in milling, in this work, a novel methodology based on Spline-Based Local Mean Decomposition (SB-LMD) and Artificial Neural Network (ANN) is proposed.

Method For this purpose, experimentally acquired audio signals in milling operation have been processed using a SB-LMD technique to extract tool chatter features. Furthermore, three ANN training algorithms viz. Resilient Propagation (RP), Conjugate Gradient Based (CGP) and Levenberg–Marquardt Algorithm (LM) and two activation functions viz. Hyperbolic Tangent Sigmoid Transfer Function (TANSIG) and Log Sigmoid Transfer Function (LOGSIG) has been used to train the data set. Among these training algorithms and activation functions, most suitable combination has been selected and further invoked to develop prediction model of chatter severity in terms of Chatter Index (CI).

Results Results showed that the proposed methodology is quite suitable for ascertaining the stable milling parameters that will result in higher productivity along with better surface finish.

Conclusion A technique to extract chatter frequency corresponding to the tool chatter has been developed and tested. Moreover, TANSIG with optimal neurons in hidden layer is found to be the most suitable one for the prediction of CI with an average deviation of 3.11%.

Keywords ANN training algorithm · Activation function · Signal processing · SB-LMD · Stability

Introduction

Regenerative chatter is a regular and complicated phenomenon that occurs frequently during machining operations. Chatter is not directly dependent on the machining parameters rather relies on the combination of these parameters. Therefore, it is quite pertinent that a proper combination of input parameters should be selected so that machining at these combinations will result in minimum chatter and maximum MRR.

In the last few decades, researchers are using process-based approach to identify chatter. In this regard, first step is to acquire the signal to identify the machining state. To achieve this, researchers have used various sensors like dynamometers [1–3], accelerometers [4–6], microphone [7–11] and Motor current [12, 13] for acquiring the signal. Delio et al. [7] compared acceleration sensors, displacement sensors with microphone, and deduced that chatter detection using acoustic signal are more effective and less costly.

The analysis of the experimentally recorded signals is the next step in tool chatter recognition. To examine the signal, some researchers employed time–frequency analysis such as Short-Time Fourier Transform (STFT) [14, 15], Continuous Wavelet Transform (CWT) [16, 17], Wavelet Transform (WT) [18, 19] and Wigner-Ville Distribution (WVD) [20]. However, due to the constraints of uncertainty principle, time–frequency methods are not so accurate. Flaws related to time–frequency analysis have been also reported in the previous literature [21].

To overcome such issues, researches have proposed various novel Self-Adaptive techniques such as Empirical

✉ Rohit Mishra
  rohitmishra2288@gmail.com

1 Jaypee University of Engineering and Technology, A-B Road, Raghogarh, Guna, Madhya-Pradesh 473226, India

Mode Decomposition (EMD) [22] and Ensemble Empirical Mode Decomposition (EEMD) [5, 6], Empirical Wavelet Transform (EWT) [23] and Variational Mode Decomposition (VMD) [24]. However, all these Self-Adaptive signal processing techniques have their own limitations such as EMD and EEMD is known for limitations like end effect, mode aliasing, sensitivity to noise and sampling. In VMD method, mode numbers must be indicated in advance [25]. EWT can lead to an improper segmentation in the frequency domain [26, 27]. To address the difficulty of EMD, a new self-adaptive signal processing techniques i.e., LMD was proposed by smith [28]. To smooth the original local mean function and envelope estimate function, the LMD process employs the moving averaging algorithm. However, LMD has also some inherent defects [29]. Recently, Mishra et al. [11] used Spline-Based Local Mean Decomposition (SB-LMD) technique to detect tool chatter in milling process using statistical indicators.

After signal processing and feature extraction, it is quite essential to develop a chatter severity model which can ensure better surface finish. In the present competitive and time-driven scenario, industries need a reliable cutting parameter for having minimum chatter. In the recent years, neural network approach has been applied to monitor machining processes [30–32]. Lamraoui et al. [33] adopted neural network approaches for chatter detection in milling. Kumar and Singh [34] employed an Artificial Neural Network (ANN) technique to forecast the safe cutting zone and metal removal rate in turning. Main concern in ANN modelling is to select the training function and optimized number of neurons in the hidden layer, to prevent it from overfitting and under fitting. However, several researchers have made an attempt to optimize the neurons in the hidden layer [35, 36].

Still, a clear concept is still missing regarding the selection of optimal neurons and the training function for applying ANN approach to build chatter severity model in terms of input milling parameters. In the present work, an attempt has been made to overcome these issues. Moreover, audio signals obtained during milling have been processed using SB-LMD technique. The remaining paper is organized as follows: Sect. 2 enumerates the outline of the presented work. Section 3 presents chatter signal simulation model. In Sect. 4, mathematical background SB-LMD is presented. Section 5 comprises the experimental details on extraction of tool chatter features. ANN modelling of chatter severity and details related to selection of optimized neuron in hidden layer and training and activation function is presented in Sect. 6. Result and discussion is presented in Sect. 7. At last, the conclusions drawn are summed up in Sect. 8.

Outline of the Presented Work

Figure 1 presents the outline of the presented work. The presented work has been divided into four stages for easy comprehension. The machine, tool, workpiece and cutting parameters have been selected in the first stage. Audio signals have been acquired using the microphone. In the second stage, viability of proposed signal processing technique i.e., SB-LMD has been tested on acquired audio signals. Normalized energy ratio (NER) and Co-relation coefficient (CC) are employed to choose the most prominent product function (PF) having higher information of tool chatter. Moreover, a new Chatter Indicator (CI) has been developed to differentiate the state of machining condition. In the third stage, An ANN model has been developed for CI using optimized neuron in hidden layer and training function.

Chatter Signal Simulation Model

In the present section, the frequency domain has been used to simulate real time working using Zeroth-Order Approximation (ZOA) [37] as shown in Fig. 2. 'N' number of teeth has been taken at milling cutter with a zero-helix angle at angular speed (Ω) (rad/s) and having cutter rotation period as 'T'. Any arbitrary tooth number (let say k) has been selected for developing the model of end milling cutter displacement. In this context, the variation of tooth engagement angle is represented by $\theta_k(t) = \Omega t$ where (Ω) (rad/s), is the angular speed of spindle. Resultant chip thickness is given by

$$h(\theta_k) = \left[f_t \sin\theta_k + \left(z_{k,0} - z_k \right) \right] u(\theta_k). \tag{1}$$

Resultant chip thickness is a combination of the static chip thickness ($f_t \sin \theta_k$) and dynamic chip thickness. Where, feed rate per tooth is represented by f_t and displacement of the cutter at the previous and present tooth periods is given by ($z_{k,0}, z_k$). Because static chip thickness does not contribute much in regenerative phenomenon, it has been omitted from the calculation. Now, modified chip thickness in terms of 'x' and 'y' direction displacement can be written as:

$$h(\theta_k) = \left[\Delta x \sin \theta_k + \Delta y \cos \theta_k \right] u(\theta_k). \tag{2}$$

The mechanistic cutting forces are directly proportional to the dynamic chip thickness and are defined in matrix form as:

$$\left\{ \begin{array}{c} F_x \\ F_y \end{array} \right\} = \frac{1}{2} b K_t \begin{bmatrix} d_{xx} & d_{xy} \\ d_{yx} & d_{yy} \end{bmatrix} \left\{ \begin{array}{c} \Delta x \\ \Delta y \end{array} \right\}, \tag{3}$$

where b, K_t and K_r are axial depth of cut and the cutting coefficients, respectively. Time-varying directional dynamic milling force coefficients are gives as

Fig. 1 Outline of the presented work
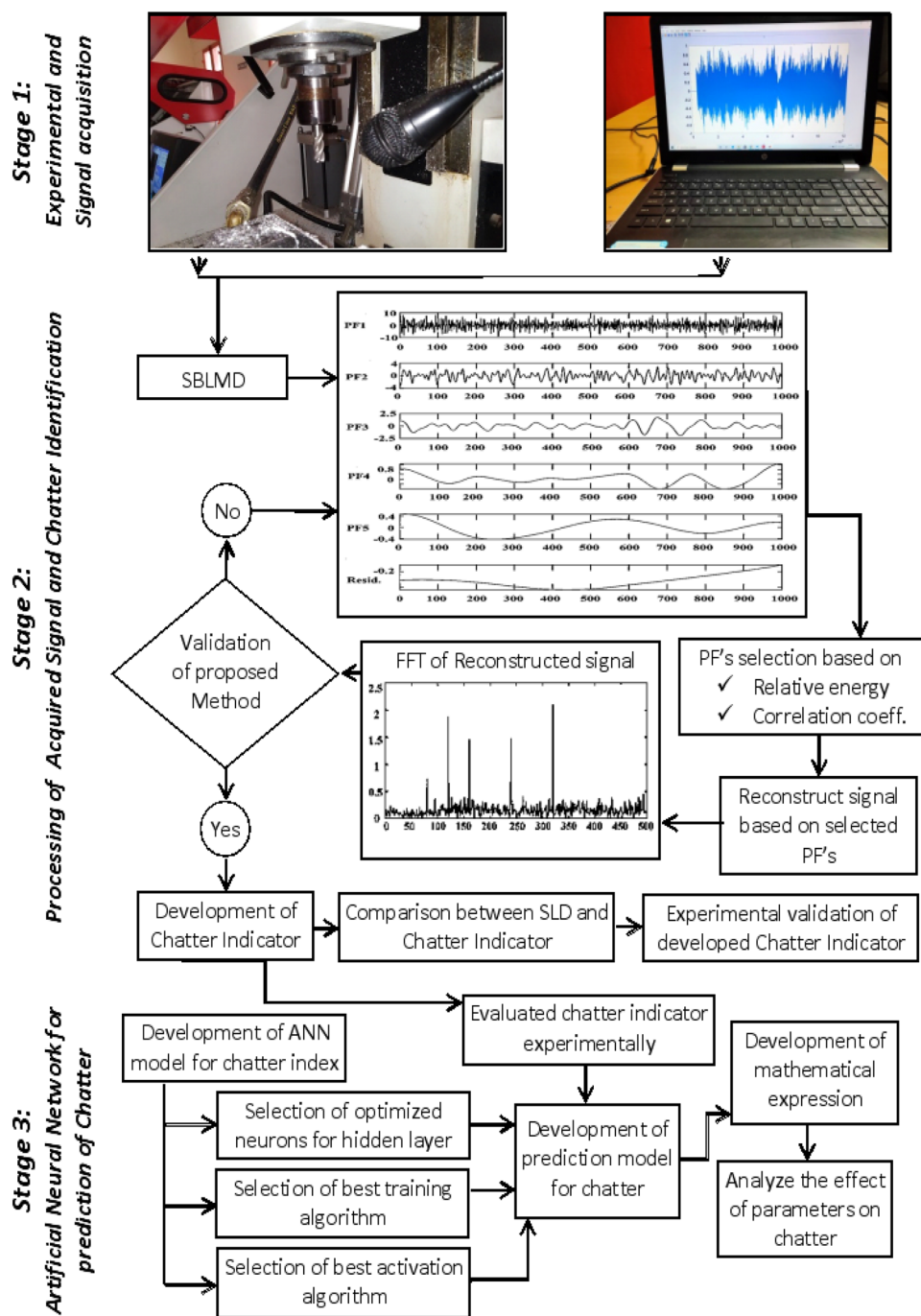
$$d_{xx} = \sum_{k=0}^{N-1} \left[K_r(1 - \cos 2\theta_k) + \sin 2\theta_k \right](-u_k); \, d_{xy} = \sum_{k=0}^{N-1} \left[K_r \sin 2\theta_k + (1 + \cos 2\theta_k) \right](-u_k)$$

$$d_{yx} = \sum_{k=0}^{N-1} \left[-K_r \sin 2\theta_k + (1 + \cos 2\theta_k) \right](u_k); \, d_{yy} = \sum_{k=0}^{N-1} \left[-K_r(1 + \cos 2\theta_k) + \sin 2\theta_k \right](u_k).$$
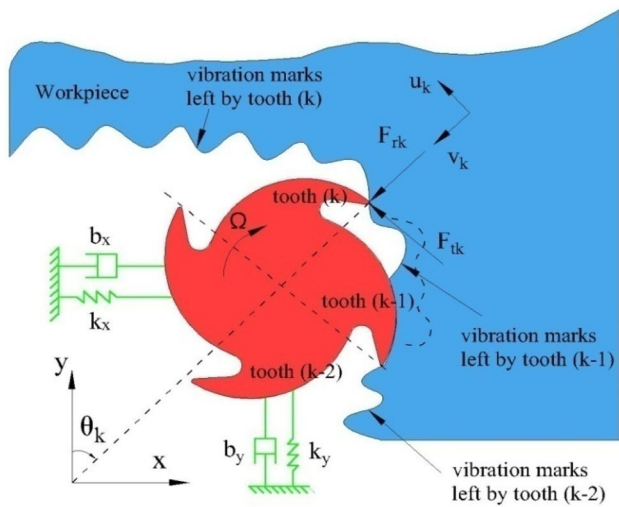
Fig. 2 Regenerative chatter in milling system

Fig. 3 Simulated signal with white Gaussian noise in time domain

$$[D(t)] = \sum_{r=-1}^{+1} [D_r]\, e^{ir\omega_T t} \tag{7}$$

White Gaussian noise has been added in the simulated model in order to realize the real working condition signal as represented in Fig. 3. This real working signal has been developed taking N (number of teeth) = 4, cutting coefficients K_t and K_r are 796 N/mm^{2}and 0.212, respectively.

Equation (3) can be expressed in the time domain matrix, given by;

$$\{F(t)\} = \frac{1}{2} b K_t [D(t)]\} \tag{4}$$

Applying Fourier transform, Eq. (4) can be expanded into the Fourier series as follows:

$$\left.\begin{aligned} [D(\omega)] &= \mathcal{F}[D(t)] = \sum_{r=-\infty}^{+\infty} [D_r]\delta(\omega - r\omega_T) = \sum_{r=-\infty}^{+\infty} [D_r]e^{ir\omega_T t}\\ [D_r] &= \frac{1}{T}\int_0^T [D(t)]e^{-ir\omega_T t}dt \end{aligned}\right\}, \tag{5}$$

where $\mathcal{F}$ and δ are the Fourier and Dirac delta function, respectively. Tooth engagement angle is given by $\theta_k = \theta + k\theta_p$ and cutter pitch angle is $\theta_p = {}^{2\pi}/_N$.

After substituting $\omega_T t = N\theta$, the directional matrix is given by

$$\begin{aligned} &= \frac{1}{\Omega T}\sum_{k=0}^{N-1}\int_{k\theta_p}^{(k+1)\theta_p}\begin{bmatrix} d_{xx,k} & d_{xy,k}\\ d_{yx,k} & d_{yy,k}\end{bmatrix}e^{-irN\theta}\\ &= \frac{1}{\theta_p}\left(\int_0^{\theta_p}\begin{bmatrix} d_{xx,0} & d_{xy,0}\\ d_{yx,0} & d_{yy,0}\end{bmatrix}e^{-irN\theta}d\theta + \int_{\theta_p}^{2\theta_p}\begin{bmatrix} d_{xx,1} & d_{xy,1}\\ d_{yx,1} & d_{yy,1}\end{bmatrix}e^{-irN\theta}d\theta + ...\right)\\ &= \frac{N}{2\pi}\int_0^{2\pi}\begin{bmatrix} d_{xx} & d_{xy}\\ d_{yx} & d_{yy}\end{bmatrix}e^{-irN\theta}d\theta. \end{aligned} \tag{6}$$

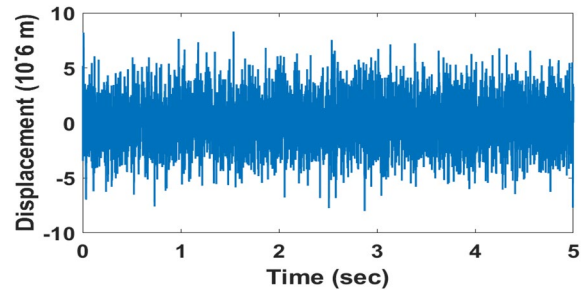When number of harmonics, $r = 0, \pm 1$, then directional coefficient matrix becomes;

Proposed Signal Processing Techniques

In the present work, an effort has been made to overcome the limitations of conventional LMD (C-LMD) by using spline interpolation. In this proposed signal processing technique, cubic spline interpolation has been used instead of moving average interpolation. Details of cubic spline interpolation has been given in ensuing section:

Cubic Spline Interpolation

Consider the problem of interpolating between the data points $(x_0, y_0), (x_1, y_1)...(x_n, y_n)$ by means of spline fitting.

Then, the cubic spline $f(x)$ must follow listed conditions:

i. $f(x)$ is a linear polynomial outside the interval (x_0, x_n),
ii. $f(x)$ is a cubic polynomial in each of the subintervals,
iii. $f'(x)$ and $f''(x)$ are continuous at each point.

Since $f(x)$ is cubic in each of the subintervals then $f''(x)$ shall be linear.

Taking equally spaced values of x so that $x_{i+1} - x_i = h$, we can write

$$f''(x) = \frac{1}{h}\left[(x_{i+1} - x)f''(x) + (x - x_i)f''(x_{i+1})\right] \tag{8}$$

Integrating twice, we have

$$f(x) = \frac{1}{h}\left[\frac{(x_{i+1} - x)}{3!}f''(x) + \frac{(x - x_i)}{3!}f''(x_{i+1})\right]a_i(x_{i+1} - x) + b_i(x - x_i) \tag{9}$$

The constants of integration a_i, b_i are determined by substituting the values of $y = f(x)$ at x_i and x_{i+1}. Thus,

$$a_i = \frac{1}{h}\left[y_i - \frac{h^2}{3!}f''(x_i)\right], b_i = \frac{1}{h}\left[y_i - \frac{h^2}{3!}f''(x_{i+1})\right]$$

Substituting the values of a_i, b_i and writing $f''(x_i) = M_i$, Eq. 9 takes the form

$$f(x) = \frac{(x_{i+1} - x)^3}{6h}M_i + \frac{(x - x_i)^3}{6h}M_{i+1} + \frac{x_{i+1} - x}{h}\left(y_i - \frac{h^2}{6}M_i\right) + \frac{x - x_i}{h}\left(y_{i+1} - \frac{h^2}{6}M_{i+1}\right) \tag{10}$$

$$\therefore f'(x) = -\frac{(x_{i+1} - x)^2}{2h}M_i + \frac{(x - x_i)^2}{6h}M_{i+1} - \frac{h}{6}(M_{i+1} - M_i) + \frac{1}{h}(y_{i+1} - y_i)$$

To impose the condition of continuity of $f'(x)$, we get. $f'(x - \varepsilon) = f'(x + \varepsilon)$ as $\varepsilon \to 0$

$$\therefore \frac{h}{6}(2M_i + M_{i-1}) + \frac{1}{h}(y_i - y_{i-1}) = -\frac{h}{6}(2M_i + M_{i+1}) + \frac{1}{h}(y_{i+1} - y_i)$$

$$M_{i-1} + 4M_i + M_{i+1} = \frac{6}{h^2}(y_{i-1} - 2y_i + y_{i+1}), i = 1.....(n - 1)$$

There are only $(n - 1)$ terms but the unknown parameters are $(n + 1)$. To get the remaining terms, the first derivative values at endpoints has been used, which are known constants. Substituting the value of M_i in Eq. 10, gives the concerned cubic spline.

Spline-Based Local Mean Decomposition (SB-LMD)

The aforementioned cubic spline interpolation has been invoked to overcome the limitation of covential LMD (C-LMD) method. Details of step followed in the SB-LMD are presented in Fig. 4.

Simulated Chatter Signal Processing via C-LMD

To test the feasibility of the proposed signal processing technique, first, a simulated chatter signal was developed (details given in Sect. 3) and has been processed with conventional LMD (C-LMD). The frequencies of the obtained simulated signal are extracted using C-LMD. The simulated chatter signal is decomposed by C-LMD into a sequence of PFs, as shown in Fig. 5a, and the corresponding Fast Frequency Transform (FFT) of PFs is shown in Fig. 5b. It is evident from these figures that the original signal's frequency peaks are not obtained.
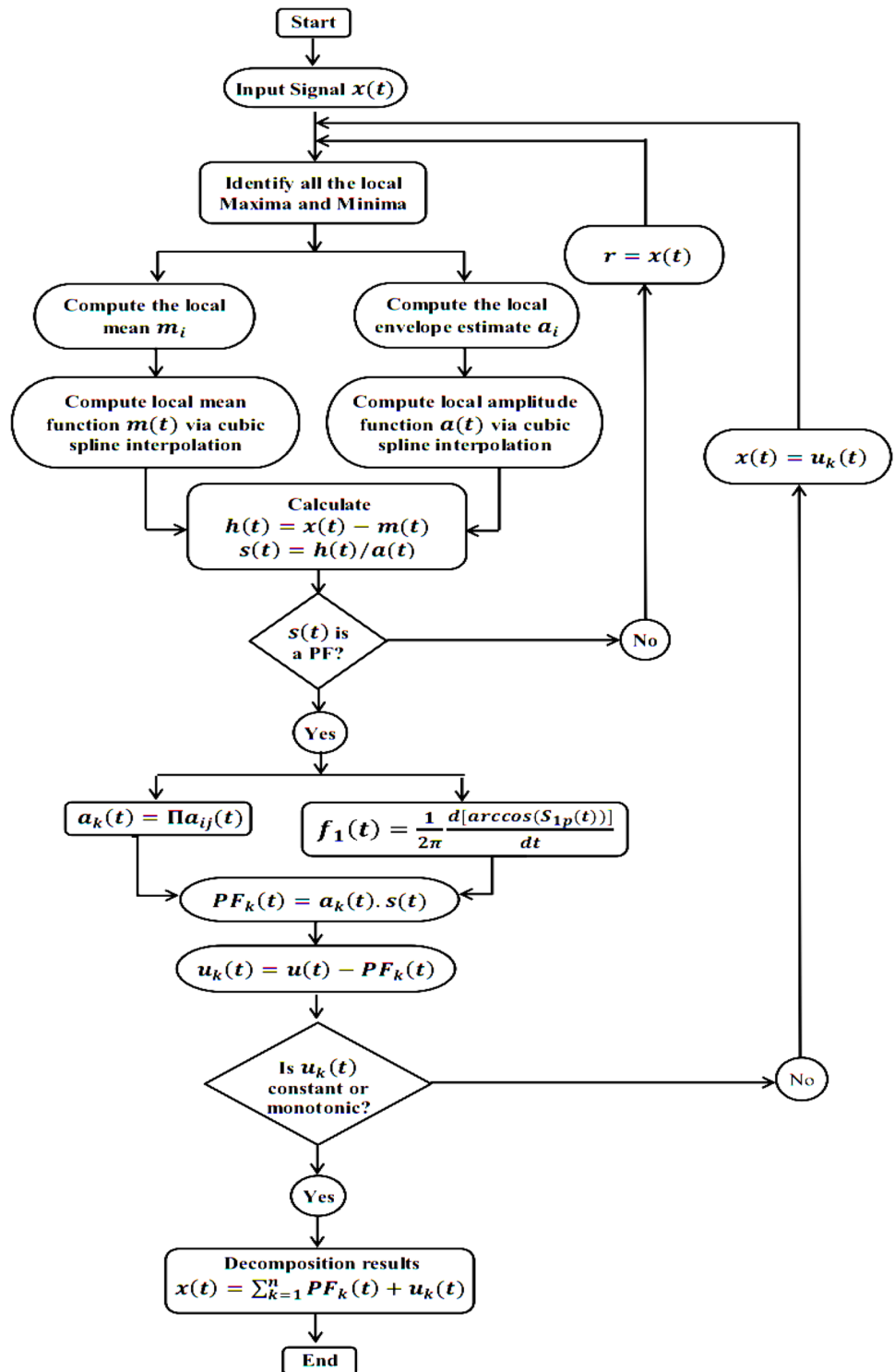
Simulated Chatter Signal Processing via SB-LMD

It is evident from the above discussion that the conventional LMD method is not always appropriate for processing a non-stationary and non-linear signal. To address the disadvantage of conventional LMD, SB-LMD is used. The PF's of the simulated chatter signal has been decomposed as shown in Fig. 6a and the corresponding FFT of first three PF's is shown in Fig. 6b. Chatter frequencies peaks are evidently marked in Fig. 6b. As a result, it can be concluded that the SB-LMD procedure is ideal for processing a non-stationary and non-linear signal signals.

Experimental Setup

End milling experiments (slotted) is performed after validating the proposed signal processing technique (SB-LMD) for simulated chatter signal. For performing the experiments, four fluted HSS milling cutter and Al 6061-T6 as a work piece material has been selected. Experimental set-up is

Fig. 4 Flowchart of SB-LMD

Start

Input Signal $x(t)$

Identify all the local Maxima and Minima

Compute the local mean m_i

Compute the local envelope estimate a_i

$r = x(t)$

Compute local mean function $m(t)$ via cubic spline interpolation

Compute local amplitude function $a(t)$ via cubic spline interpolation

$x(t) = u_k(t)$

Calculate
$h(t) = x(t) - m(t)$
$s(t) = h(t)/a(t)$

$s(t)$ is a PF? — No

Yes

$a_k(t) = \Pi a_{ij}(t)$

$f_1(t) = \dfrac{1}{2\pi}\dfrac{d[arccos(S_{1p}(t))]}{dt}$

$PF_k(t) = a_k(t).s(t)$

$u_k(t) = u(t) - PF_k(t)$

Is $u_k(t)$ constant or monotonic? — No

Yes

Decomposition results
$x(t) = \sum_{k=1}^{n} PF_k(t) + u_k(t)$

End

shown in Fig. 7. Microphone (Model No: AHUJA AGN-480) having 600 Ω impedance and 2 mV/Pa sensitivity, has been used for gathering the generated sound signals (real working signal) during machining. Total 27 experiments have been performed with full factorial combinations of the input parameters, as presented in Table 1. Figure 8 shows a sample audio signal generated during a milling operation with an axial depth of cut of 1 mm, a feed rate of 50 mm/min, and a spindle speed of 1000 rpm.

Fig. 5 **a** C-LMD processed simulated chatter signal, and **b** FFT of first three PF's
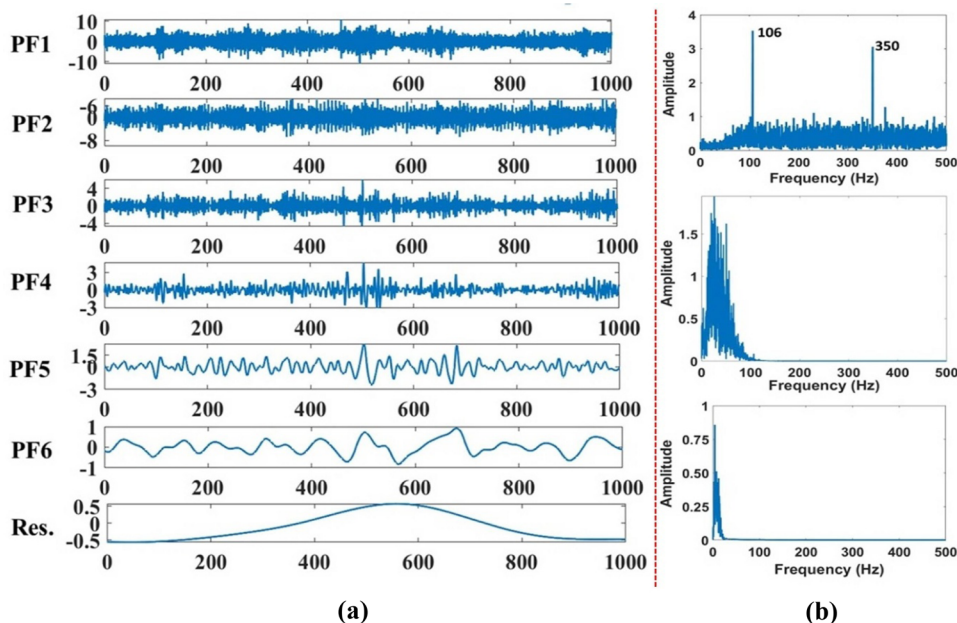
Fig. 6 **a** SB-LMD processed simulated chatter signal, and **b** FFT of first three PF's
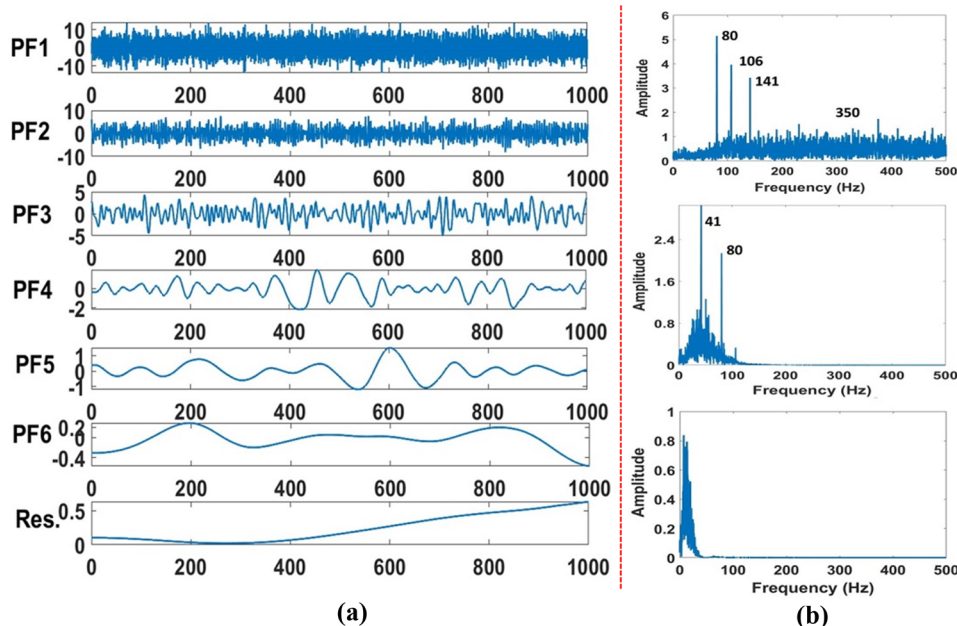

SB-LMD in Real Working Signals

For extracting the valuable components and removing the time series and associated spatial noise components from sound signal, SB-LMD technique is applied. Extracted Product Functions (PF's) of the signal are shown in Fig. 9. Two major indicators are introduced to pick the important PF's, containing the principle data of processing state. Relative energy ratio (NER) of the foremost noticeable PF shows higher energy content. When cutting is steady, energy dispersion is uniform and relative energy ratio is small. However, when chatter starts, relative energy ratio increases. Therefore, relative energy ratio is a good indicator to select the crucial PF's. Second indicator, co-relation coefficients (CC) is also used.

The first three PFs have a higher relative energy ratio as well as higher correlation coefficient, as shown in Fig. 10. Therefore, first three PF's are used to constitute the main signal information.

Figure 11 displays the newly developed signal's frequency spectrum. It is evident from Fig. 11 that SB-LMD technique is able to extract all three basic important frequency

Fig. 7 End milling experimental set-up
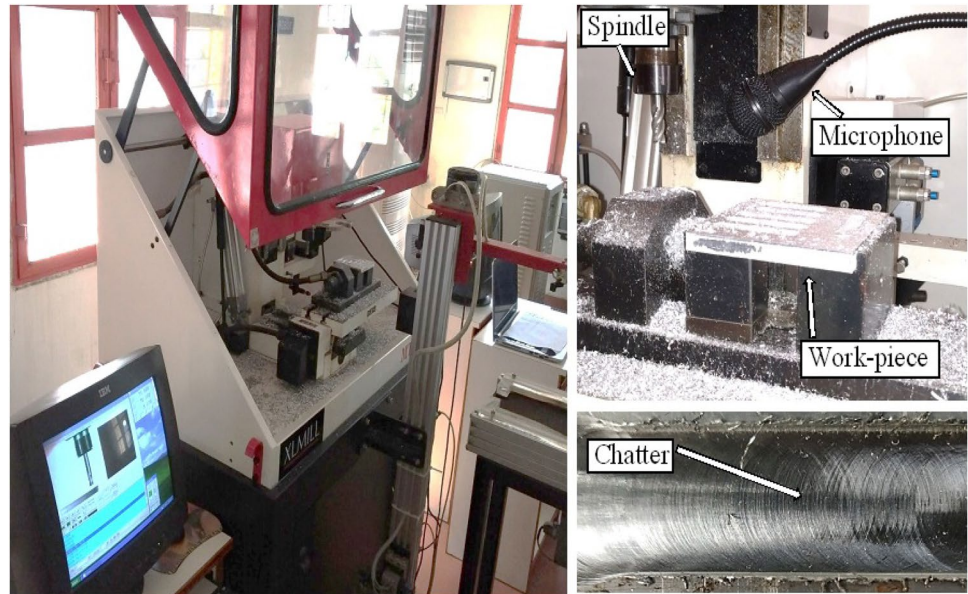
Table 1 Experimental setting (3 parameters at 3 levels)

Parameters	Level 1	Level 2	Level 3
Spindle speed (SS, rpm)	1000	2000	3000
Feed rate (F, m/min)	50	75	100
Axial depth of cut (D, mm)	1	1.5	2
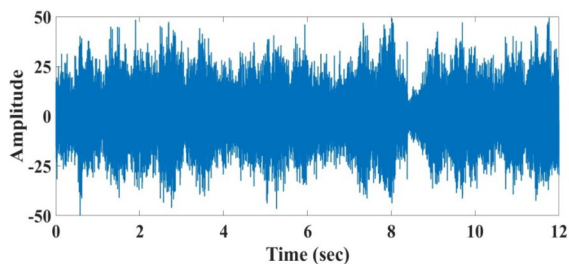
Fig. 8 Sound signals for test run 1

components, i.e., chatter frequency, tooth passing frequency ($\omega_T = 66.6$ Hz) and multiples of tooth passing frequency (ω_k).

Extraction of Tool Chatter Features

For ANN modelling, tool features are required. Therefore, in this section, SB-LMD processed audio signals are further explored by employing a new statistical indicator, Chatter Indicator (*CI*). Chatter Indictor is based on coefficient of variation, i.e., the ratio of mean to the standard deviation given by following relation:

$$CI = \frac{\text{Mean } (\bar{x})}{\text{Standard deviation } (\sigma)} . \tag{12}$$

Coefficient of variation is employed, because it reflects the degree of variability in proportion to the mean of the sound data point. Therefore, the value of *CI* is directly proportional to signal's chatter components. *CI* is calculated for each of the 27 experimental runs and presented in Fig. 12.

For all 27 experimental runs, the variation of *CI* has been calculated and marked in Fig. 12. Upper (red) and lower (green) threshold limits are defined using 3σ criterion to classify the three phases of chatter severity (stable, moderate and unstable), as demonstrated in Fig. 12. Green line represents the stable machining, while *CI* points above the red line represents unstable machining. The points in the middle (between green and red) represent a transition from stable to unsafe machining.

Surface topography of the machined surface was carefully studied at experimental runs 7 and 27, as shown in Fig. 13a, b, respectively, to understand the effect of feed rate. When looking at the surface topology of machined surfaces, it is obvious that clear and distinct chatter marks can be seen.

Artificial Neural Network

Furthermore, a suitable prediction model has been created to investigate the relative dependency of chatter severity in terms of input milling parameters. Thus, to meet this objective, ANN technique has been invoked as presented in the present section.
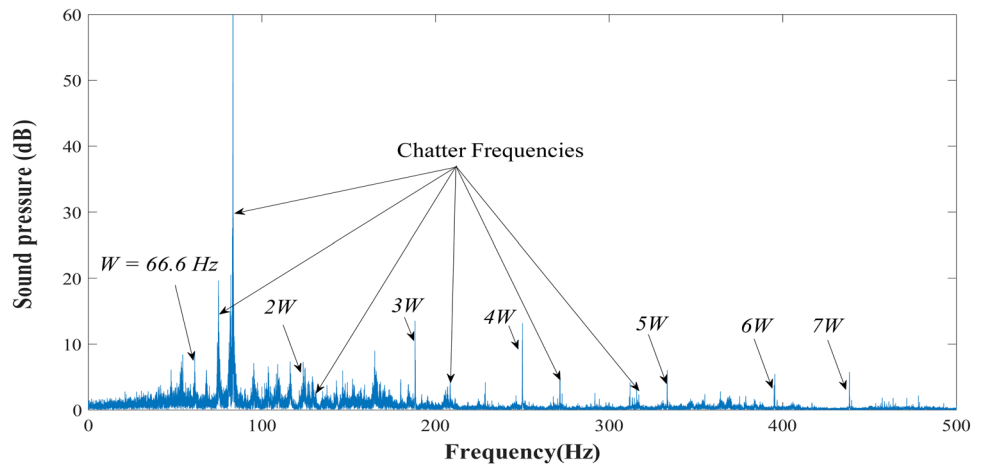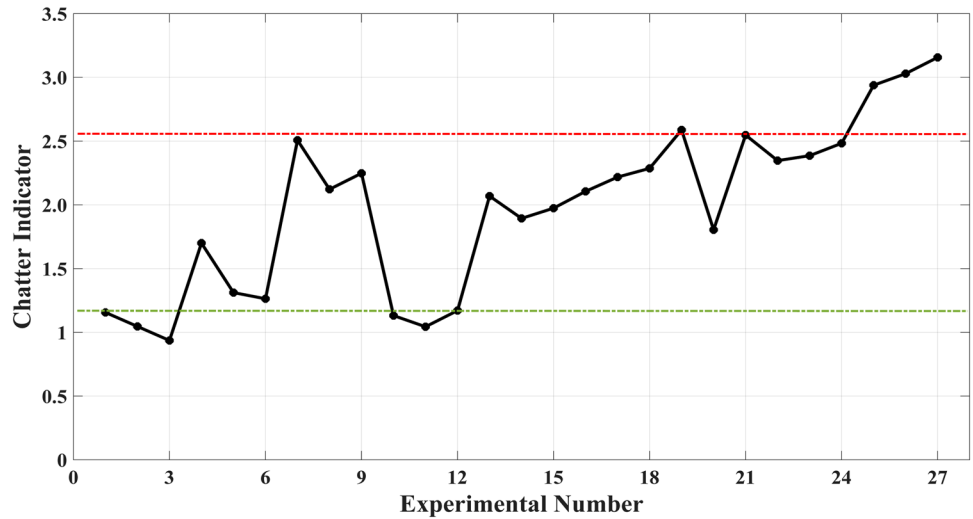
Fig. 9 SB-LMD processed real chatter signal
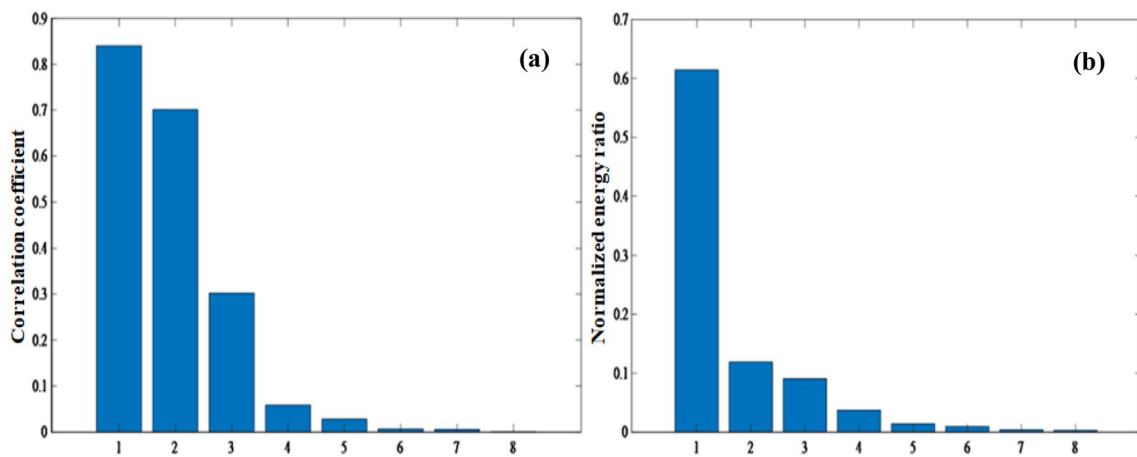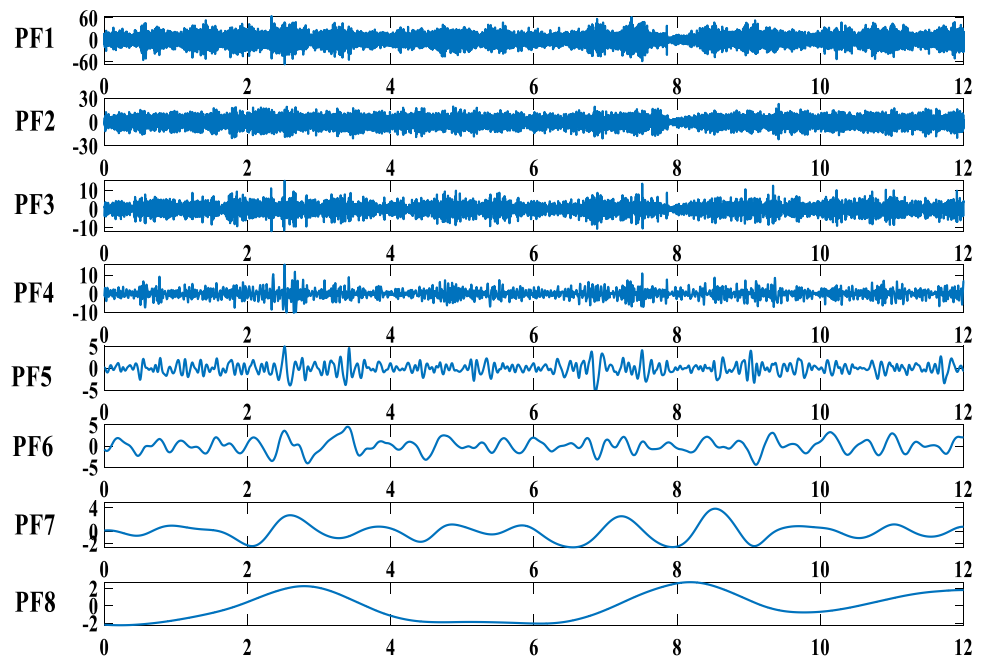
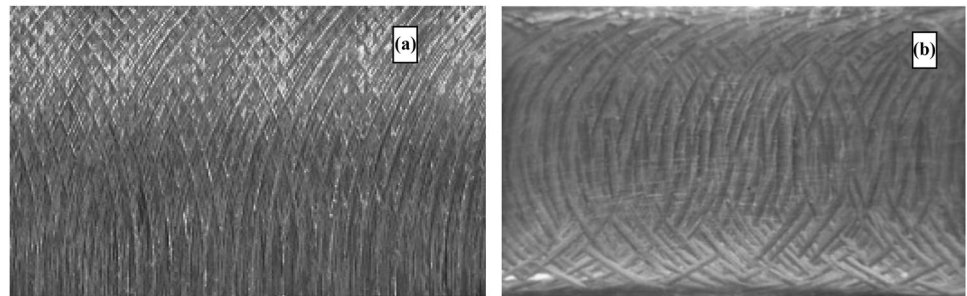**Fig. 10** **a** CC and **b** NER of PF's

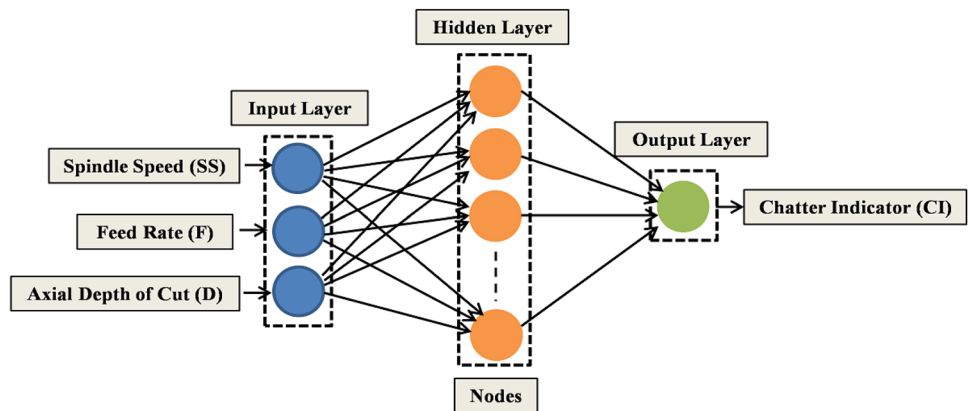**Fig. 11** FFT of reconstructed signal

Fig. 12 Coefficient of variation (*CI*) v/s experimental number

Fig. 13 Surface topology for (**a**) experiment 7 and (**b**) Experiment 27

Fig. 14 ANN architecture

Overview and Architecture of Artificial Neural Network

The human brain and biological nervous system are the cause of motivation behind the development of artificial neural network. Artificial neurons in ANN are the simplified models of biological neurons that are used for computational or processing the data. In the present work, architectures of ANN considered consists of three layers viz. Input [having 3 neurons, 'Spindle Speed (*SS*)', 'Feed Rate (*F*)' and 'Axial Depth of Cut (*D*)'], hidden (having optimized number of neurons) and output layer [one neuron, i.e. 'Chatter Indicator (*CI*)'] as shown in Fig. 14. Input layer receives machining data from the user end. Hidden layers perform most of the complex processing for extracting the features. An output layer presents the final output.

In ANN modelling, various training functions are available and can be used for training the data. Viability of

training function is problem specific. In this work, different variants of BP algorithms have been invoked for training the model to improve the efficiency of ANN for producing better prediction models for chatter identification. To enhance the efficiency of back propagation in terms of its convergence, several algorithms have been developed known as variants of Back propagation. The variants of BP algorithms are as follows:

a) Resilient Propagation (RP).
b) Conjugate Gradient-based Algorithms (CGP).
c) Levenberg–Marquardt Algorithm (LM).

To improve the prediction capability of ANN, different activation function has been used. List of activation functions are as follows:

a) Hyperbolic tangent sigmoid transfer function (TANSIG) $= \frac{2}{1+e^{-2z}} - 1$
b) Log sigmoid transfer function (LOGSIG) $= \frac{1}{1+e^{-z}}$
c) Linear transfer function (PURELIN) $= z$

In this study, PURELIN function has been discarded due to linear property which does not meet with the required condition.

To compare the above listed training (RP, CGP and LM) and activation function (TANSIG and LOGSIG) has been taken in consideration for better prediction of chatter and their details are given in sub sequent sections. In this study, an effort has been done to get the optimized neurons for the selected training and activation function to avoid the case of under or over fitting of the prediction model. Later, these optimized neurons for hidden layer are used to train the data. Details are given in subsequent section.

Selection of Number of Neurons in the Hidden Layer

Optimized Neuron in Hidden Layer for TANSIG

To get optimized neuron in the hidden layer for selected training function (RP, CGP and LM) and TANSIG as an activation function, Mean squared error (MSE) has been taken as a statistical indicator to select the number of neurons. To achieve the optimized neurons, data have been trained for all selected training algorithm taking TANSIG as an activation function, by varying the number of neurons in the hidden layer from 1 to 30. Mean squared error have been calculated for all these combinations. Calculated mean squared errors (MSE) have been plotted against number of neurons as shown in Fig. 15.
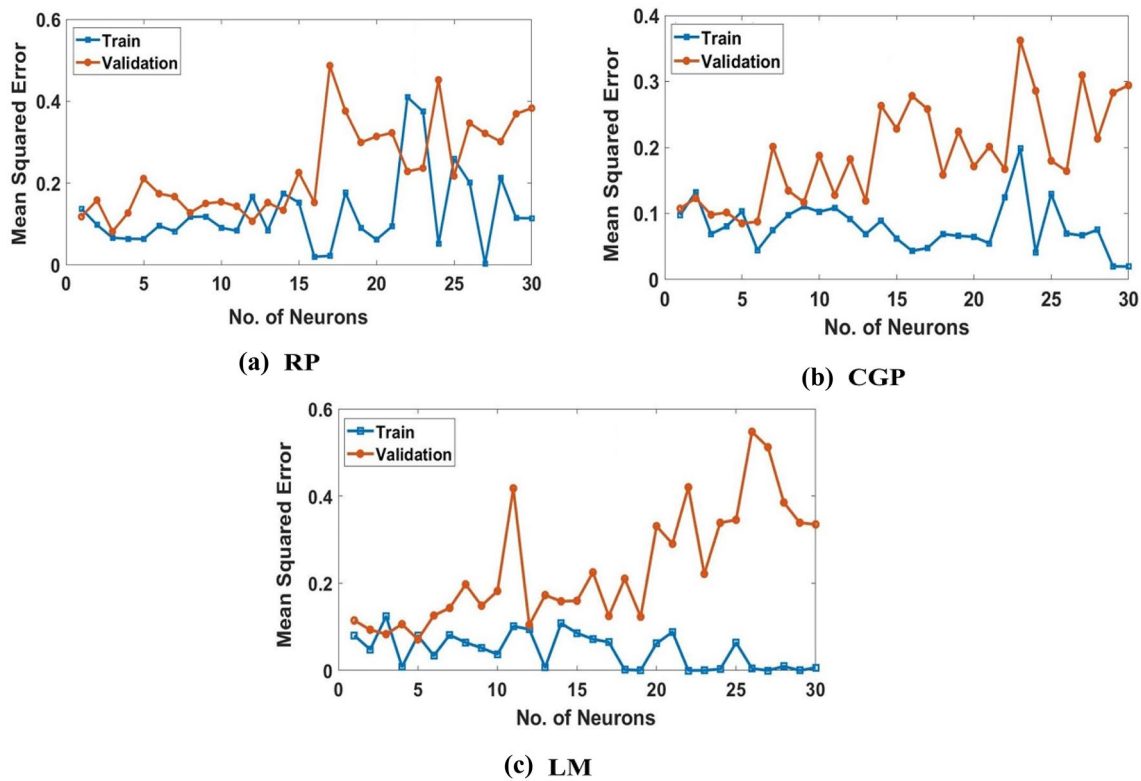

(a) RP

(b) CGP

(c) LM

Fig. 15 MSE v/s number of neurons for selected training algorithms using TANSIG
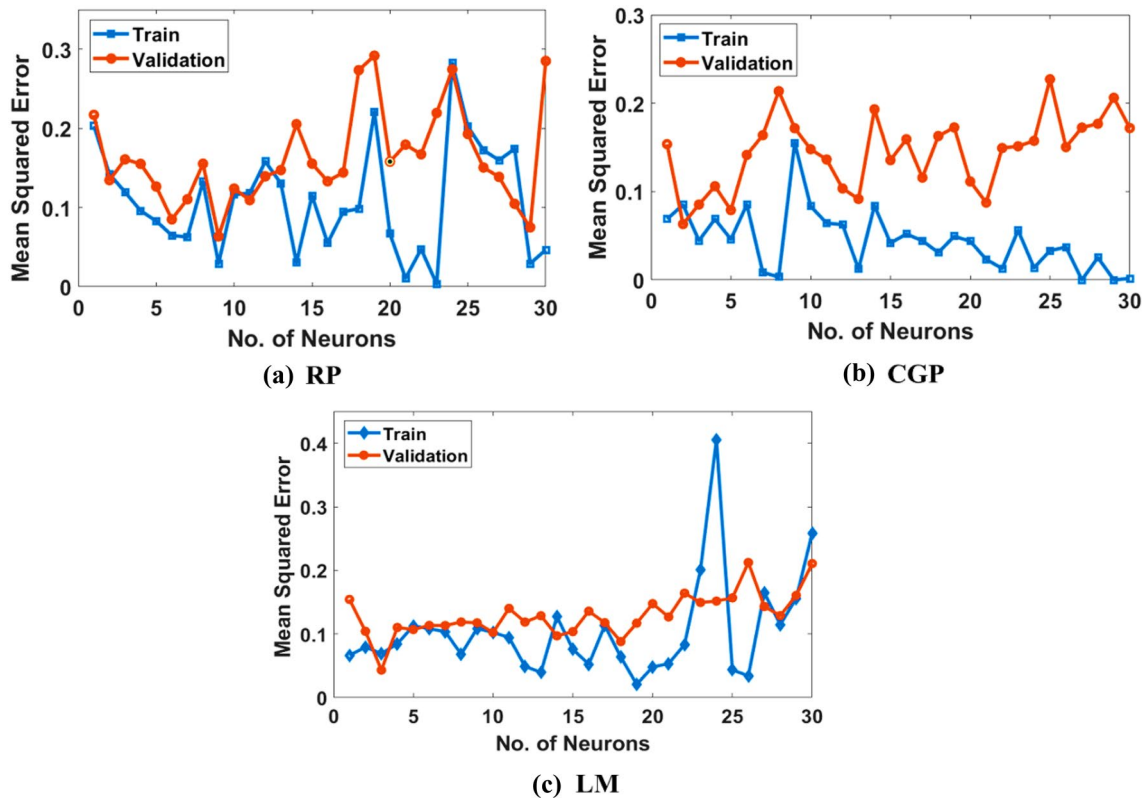
Fig. 16 MSE v/s number of neurons for selected training algorithms using LOGSIG

Form Fig. 15, it has been observed that, optimized number of neurons are different for different algorithm. Optimized numbers of neurons in hidden layer for algorithms have been decided based on minimum difference between the train data and the validation data. From Fig. 15, it is observed that the optimum number of neurons for RP, CGP and LM are 8, 9 and 5 neurons, respectively.

Optimized Neuron in Hidden Layer for LOGSIG

Similarly, optimized neurons in the hidden layer have been evaluated for selected training function (RP, CGP and LM) and LOGSIG used as an activation function as presented in above section. Calculated mean squared errors (MSE) have been plotted against number of neurons as shown in Fig. 16.

Form Fig. 16, it has been observed that, optimized number of neurons are different for different algorithm. Optimized numbers of neurons in hidden layer for algorithms have been decided based on minimum difference between the train data and the validation data. From Fig. 16, it is observed that the optimum number of neurons for RP, CGP and LM are 10, 9 and 6 neurons, respectively.

Selection of Training function

To select the best training algorithm for the prediction of chatter severity taking TANSIG and LOGSIG as an activation function, ANN model is trained individually using RP, CGP, LM algorithms. Three input parameters [i.e. Spindle speed (SS), Feed rate (F) and Axial depth of cut (D)] are used as the input neurons layer. To anticipate the chatter, the output layer has one neuron i.e., Chatter Indicator (CI). Optimized number of neurons has been for further analysis.

When compared to the depth of cut (0.5–1.5 mm) and feed rate (0.1–0.2 m/min), the spindle speed range (1000–3000 rpm) is numerically too broad. As a result, the available data set is standardised to facilitate training and testing. The normalised values are in the range of 0 to 1 in this case. When the disparity between each parameter data is too great, normalised values are employed. This allows us to compare the sizes on a common scale to identify which component has the most impact on the response. This also aids in the preservation of orthogonality. The transformation of non-normalized variables into normalized form of input and output variable has been done by using the following relations:

Table 2 AAPD for TANSIG and LOGSIG

| Exp. no	TANSIG			LOGSIG		
	RP–APD	CGP–APD	LM–APD	RP–APD	CGP–APD	LM–APD
1	12.9621	13.5288	1.00958	5.3810	6.8615	8.9649
2	4.68413	33.6529	4.45988	6.2186	21.3631	0.4194
3	14.2919	4.82969	2.91949	8.1861	13.5741	0.1977
4	5.53062	4.84434	0.19153	2.0101	0.5293	0.7037
5	3.39977	1.71631	3.82687	8.1165	1.3467	0.6945
6	6.80972	32.4499	4.68538	9.3144	15.5898	0.1505
7	19.159	2.49737	0.11753	9.3937	16.6714	5.7847
8	0.41797	16.9794	11.3136	13.6774	2.1675	2.2021
9	20.3961	13.9739	12.8057	14.3826	0.7358	0.0345
10	3.08211	10.8766	5.23235	7.4500	5.4907	3.6930
11	7.18601	20.0466	4.81344	7.5510	14.0496	4.0927
12	5.74493	15.0235	1.47986	9.4807	8.7502	1.3323
13	6.85476	11.9293	2.0317	5.1585	16.1603	6.0447
14	8.8728	5.15317	5.61925	6.3734	9.7012	4.3897
15	6.99633	2.03933	0.61758	3.7603	15.8117	0.2539
16	7.63755	20.4439	4.67509	11.7671	22.3663	0.4784
17	5.02753	3.87751	1.26141	6.0248	2.6014	0.8463
18	1.52985	7.2358	2.10819	2.2283	19.9084	0.0625
19	10.0913	24.1096	1.14889	0.5626	14.1931	51.4285
20	7.6863	13.4731	0.02033	36.6798	3.0454	1.6154
21	12.4974	19.8428	0.85464	1.6747	9.5350	0.8495
22	0.24277	1.8717	2.64737	3.0664	5.4592	1.5315
23	3.60494	9.55663	2.17567	8.7969	22.0642	1.5823
24	9.12771	2.68165	3.91282	1.6286	2.5768	1.6477
25	4.85553	9.48168	3.67377	9.5325	7.6414	1.4502
26	8.06975	30.4059	0.26709	3.2910	2.1469	0.8186
27	5.59931	9.40351	0.27276	12.1037	1.3148	2.3161
AAPD	**7.49475**	**12.6639**	**3.11636**	**7.9189**	**9.6910**	**3.8365**

Abbreviated form is presented by bold

$$SS_n = \frac{SS}{SS_{max}}; F_n = \frac{F}{F_{max}}; D_n = \frac{D}{D_{max}}; CI_n = \frac{CI}{CI_{max}}$$

Finally, the final trained network weights are those that result in the least amount of inaccuracy. To evaluate the prediction capability of the algorithms, Absolute Percentage Deviation (APD) has been calculated and presented in Table 2. Later, final Average Absolute Percentage Deviation (AAPD) has been calculated for every algorithm.

When TANSIG is used as an activation function, the Average Absolute Percentage Deviation (AAPD) for RP, CGP and LM are 7.49, 12.66 and 3.11, respectively. In LOGSIG activation function, average absolute percentage deviations for RP, CGP and LM are 7.92, 9.69 and 3.84, respectively. After comparing all possible combinations of selected training algorithm and activation functions, LM with TANSIG is found to be the most suitable combination for predicting the output (Chatter Index).

Fig. 17 ANN model
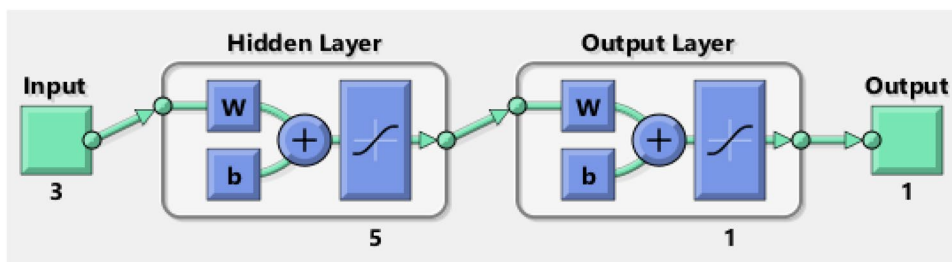
Table 3 Weight to hidden layer from input layer

Neurons	$a_1^1(ss_n)$	$a_2^1(F_n)$	$a_3^1(D_n)$	bias^1
a_1^2	0.96957	-3.1665	0.53242	-2.9347
a_2^2	-1.6207	0.14413	3.243	-1.0427
a_3^2	-2.6834	0.041645	2.333	-0.80378
a_4^2	1.3065	0.81295	1.1194	0.85065
a_5^2	0.93809	1.9373	0.96782	1.111

Prediction Model for CI

After selecting best training and activation function and optimized number of neurons in the previous sections, prediction model has been developed for CI (Chatter indicator). Proposed ANN model for CI is shown in Fig. 17. Three neurons (SS_n, F_n, D_n) in the input layer, five neurons in the hidden layer, and one neuron (CI_n) in the output layer are used to create a CI prediction model. For ANN modelling, LM algorithm as a training function along with TANSIG activation function (between the input and hidden layer) and TANSIG (between the hidden and output layer) has been used. Table 3 shows the optimal weight and bias for the hidden layer from the input layer. Table 4 shows the optimal weight and bias for the output layer from the hidden layer. For better understanding, superscript is used to represent the number of layer and subscript is used to represent the position of neuron in that layer.

Development of Mathematical Expression

To develop the mathematical expression for ANN model, θ expression has been used to represent the weight, whereas 0 is used to present the position of bias in the mathematical expression.

Mathematical expression for hidden layer is expressed as:

$$z_1^2 = \theta_{11}^1 \times a_1^1 + \theta_{12}^1 \times a_2^1 + \theta_{13}^1 \times a_3^1 + \theta_{10}^1$$
$$z_2^2 = \theta_{21}^1 \times a_1^1 + \theta_{22}^1 \times a_2^1 + \theta_{23}^1 \times a_3^1 + \theta_{20}^1$$
$$z_3^2 = \theta_{31}^1 \times a_1^1 + \theta_{32}^1 \times a_2^1 + \theta_{33}^1 \times a_3^1 + \theta_{30}^1$$
$$z_4^2 = \theta_{41}^1 \times a_1^1 + \theta_{42}^1 \times a_2^1 + \theta_{43}^1 \times a_3^1 + \theta_{40}^1$$
$$z_5^2 = \theta_{51}^1 \times a_1^1 + \theta_{52}^1 \times a_2^1 + \theta_{53}^1 \times a_3^1 + \theta_{50}^1$$

where θ (Tables 3 and 4) is the weight, θ superscript represents the connection between the layers (input to hidden layer), first number in θ subscript is representing the position of neuron in the second layer. Second number in θ subscript

is the position of neuron in the first layer. To get the value of neurons in the hidden layer, z values need to be fed in to the activation function (TANSIG).

Now, neurons in the hidden layer are calculated using the expressions;

$$a_1^2 = \frac{2}{1 + e^{-2 \times z_1^2}} - 1; a_2^2 = \frac{2}{1 + e^{-2 \times z_2^2}} - 1; a_3^2 = \frac{2}{1 + e^{-2 \times z_3^2}} - 1$$
$$a_4^2 = \frac{2}{1 + e^{-2 \times z_4^2}} - 1; a_5^2 = \frac{2}{1 + e^{-2 \times z_5^2}} - 1$$

Mathematical expression for output layer is expressed as

$$z_1^3 = \theta_{11}^2 \times a_1^2 + \theta_{12}^2 \times a_2^2 + \theta_{13}^2 \times a_3^2 + \theta_{14}^2 \times a_4^2 + \theta_{15}^2 \times a_5^2 + \theta_{10}^2$$

To get the value of neuron at the output layer, TANSIG function is used. Therefore, neuron value in the output is determined using the following expression

$$a_1^3(\text{CI}_n) = \frac{2}{1 + e^{-2z_1^3}} - 1$$

This developed mathematical expression for *CI* has been used to explore the effect of individual parameter on chatter severity. Outcome of this study has been presented in the subsequent section, i.e., result and discussion.

## Result and Discussion

Effect of Individual Parameters on CI

Effect of individual input milling parameters on Chatter Indicator (*CI*) has been studied by plotting the outputs with respect to the input parameters viz. Spindle Speed (*SS*), Feed Rate (*F*) and Axial Depth of Cut (*D*) as shown in Fig. 18. On analyzing Fig. 18a, it can be interpreted that Chatter Indicator (*CI*) increases with the increase in spindle speed. By critically analyzing blue, red and green line in Fig. 18a, it is observed that the percentage change in Chatter Indicator (*CI*) is 81.91%, 49.35% and 30.47%, respectively. Percentage change in blue line which is drawn at low feed and depth of cut (*F* = 50 mm/min and *D* = 1 mm) is higher as compared to other lines. Thus, it can be concluded that the relative effect of Spindle Speed (*SS*) is dominating at lower values of Feed rate (*F*) and Axial Depth of Cut (*D*).

From Fig. 18b, it can be inferred that Chatter Indicator (*CI*) is not so much affected by the variation in Feed Rate (F) as already discussed in Fig. 12. Moreover, the percentage change in *CI* with Feed Rate (*F*) at respective Spindle Speed;

Table 4 Weight to output layer from hidden layer

Neurons	a_1^2	a_2^2	a_3^2	a_4^2	a_5^2	bias^2
$a_1^3(CI_n)$	-0.84787	1.8025	-1.7219	2.0199	-1.8609	-0.7327

Fig. 18 Effect of milling parameters on *CI*
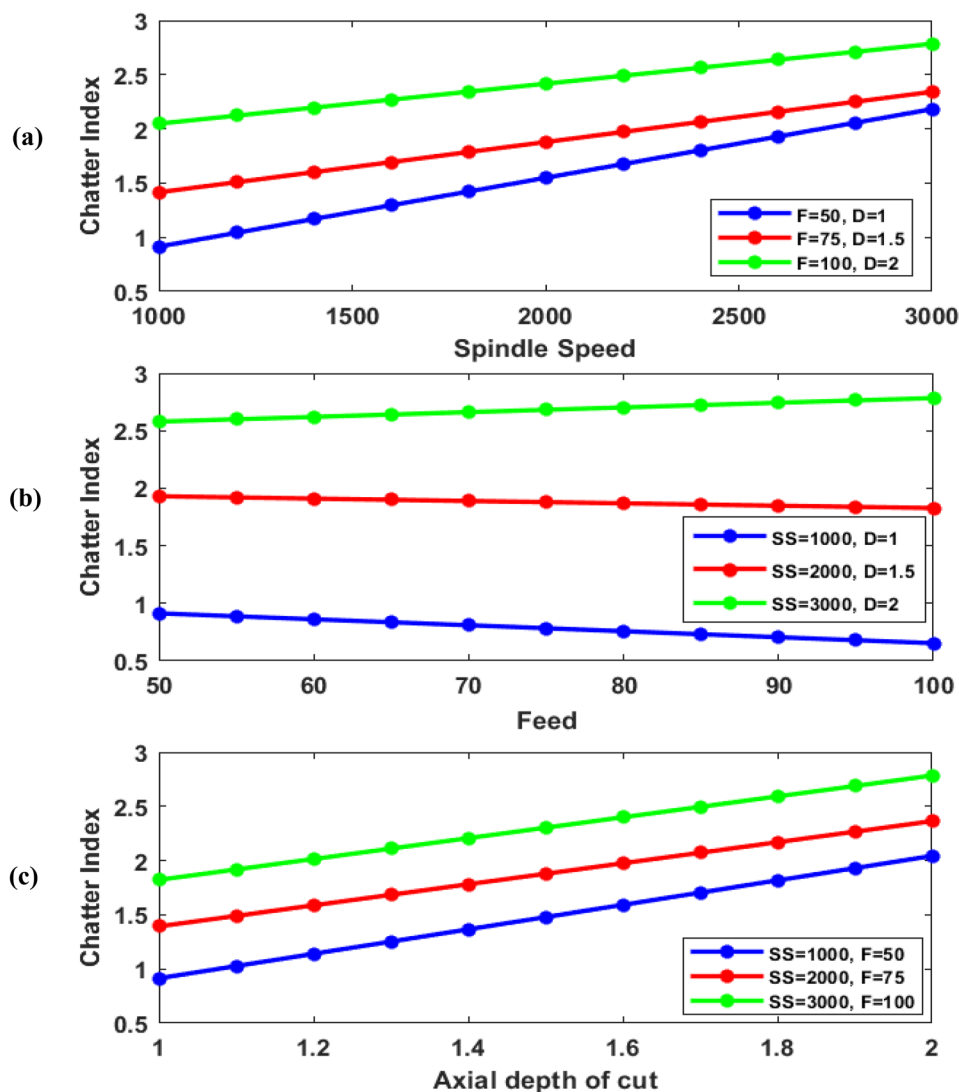
SS (1000, 2000 and 3000 rpm) and Axial Depth of Cut; *D* (1, 1.5 and 2 mm) are 33.16%, 5.46% and 7.65%, respectively. However, percentage change in CI w.r.t feed rate at low spindle speed and axial depth of cut (*SS* = 1000 rpm and *D* = 1 mm) is higher as compared to the rest two states.

In Fig. 18c, effect of Axial Depth of Cut (*D*) at constant Spindle Speed (*SS*) (1000, 2000 and 3000 rpm) and Feed Rate (*F*) (50, 75 and 100 mm/min) on Chatter Indicator (*CI*) has been shown in three colours viz. blue, red and green. By observing Fig. 18c, it can be deduced that Chatter Indicator (*CI*) increases with the increase in Axial Depth of Cut (*D*). Percentage variations Chatter Indicator (*CI*) for blue, red and green lines are 76.36%, 51.67% and 41.77%, respectively. The net differences in the value of Chatter Indicator (*CI*) for blue, red and green lines are 1.129, 0.9705 and 0.962, respectively. Thus, on comparing Fig. 18a–c, it is obvious that the effects of Spindle Speed (*SS*) and Axial Depth of Cut (*D*) on Chatter Indicator (*CI*) are more severe as compared to Feed Rate (*F*).

A similar result has also been presented earlier by analyzing Fig. 12.

Effect of interaction parameters on CI and MRR

Occurrence of chatter in milling results in poor surface finish and degraded tool life. Therefore, to maximize productivity along with better surface finish and longer tool life, it is necessary to minimize Chatter Indicator (*CI*), which ultimately depends on the interaction of input milling parameters. Therefore, the effects of interaction parameters on Chatter Index have been discussed in the present section with the help of contour and surface plots as presented in Fig. 19.

Figure 19a represents the variation of Chatter Indicator (*CI*) with respect to spindle speed and axial depth of cut at constant feed rate (75 mm/min). Figure 19b represents the variation of Chatter Index with respect to feed rate and axial depth of cut at constant spindle speed (2000 rpm).

Fig. 19 Contour and surface plots for *CI*
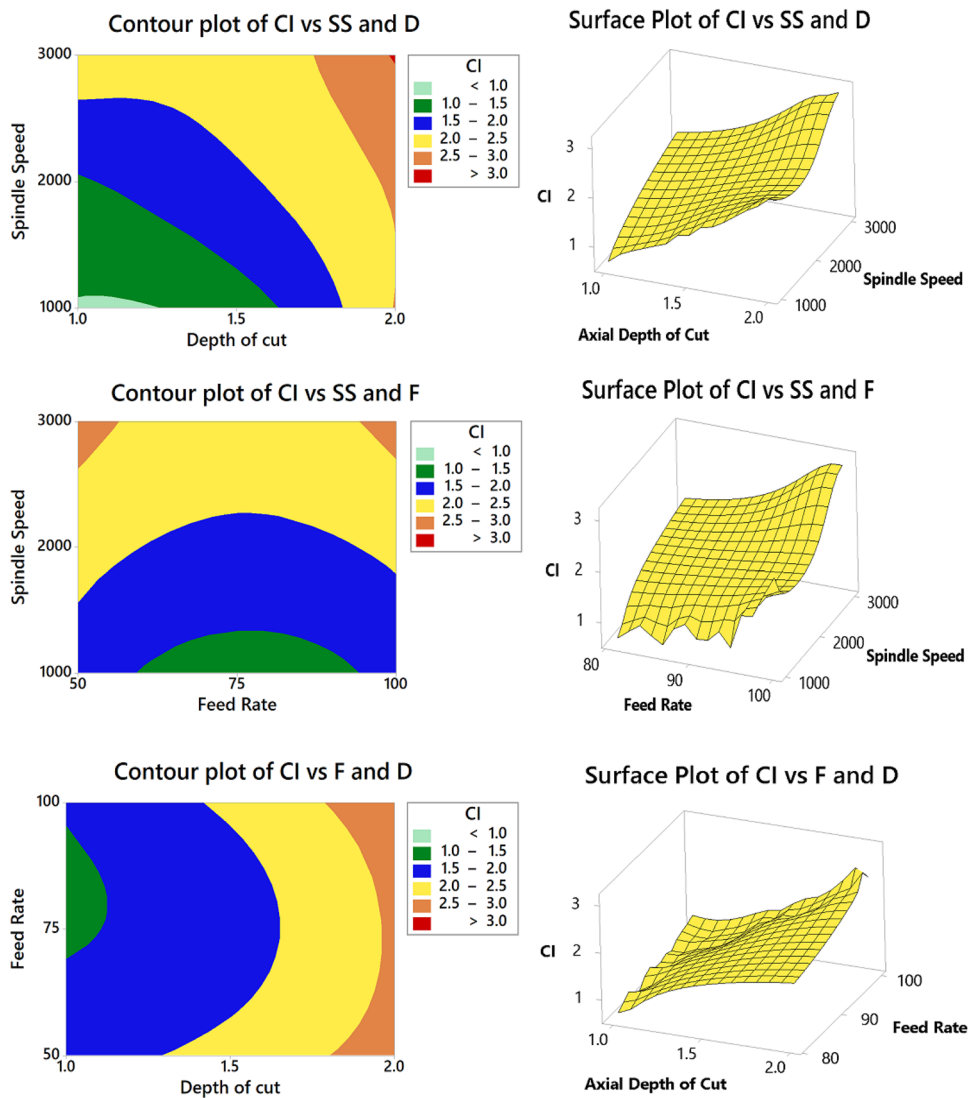
Table 5 Chatter severity regimes

Chatter severity	Chatter index
Unstable	$CI \geq 2.5$
Moderate	$2.5 > CI > 1.5$
Stable	$CI \leq 1.5$

Table 6 Stability range

	Axial depth of cut (mm)	Feed rate (m/min)	Spindle Speed (rpm)
Optimal range	1.6–1.78	81–100	2380–2900

Figure 19c represents the variation of Chatter Index with respect to spindle speed and feed rate at constant axial depth of cut (1.5 mm). These variations in Chatter Index have been presented with different colours (green, dark green, blue, yellow, tangerine and red). As colour level changes from green to red, chatter level increases. Minimum and maximum chatter within the considered range of parameters is represented by green and red colours, respectively. From these figures, it is evident that combined range of axial depth of cut, spindle speed and feed rate should be selected in such
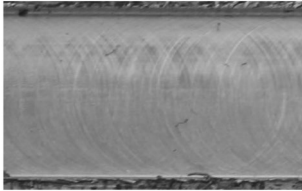
a way that it will result in minimum chatter (represented by green colour).

Finally, on collectively analyzing all these figures, favourable output range of *CI* (green colour) has been evaluated as shown in Table 5.

Safe Milling Zone

After analyzing the severity of individual parameters on chatter severity, range of parameters pertaining to stable

Table 7 Experimental validation

Exp. no	Axial depth of cut (mm)	Spindle speed (rpm)	Feed rate (mm/min)	CI	Surface view
1	1.7	2400	90	1.14	

milling have been ascertained by extracting common range of values from Fig. 19 and are presented in Table 6.

To validate the obtained range, further experiment has been performed. This experiment has been performed considering the developed stable range and is presented in Table 7. Result of validation experiment shows that at this milling range *CI* value is below the threshold stability value as shown in Fig. 12. Moreover, surface texture of the machined surface is also presented in Table 7. On examining this surface texture, it is also evident that the developed range is correct. Thus, the proposed methodology is quite suitable for ascertaining the stable milling parameters that will result in higher productivity along with better surface finish.

Conclusion

In the present work, a methodology has been proposed to ascertain tool chatter severity regimes in milling operation. A new modified LMD approach based on cubic spline interpolation and ANN modelling has been used to achieve the aforementioned objective. Moreover, to explore the influence of input milling parameters on chatter severity, ANN modelling has been invoked. Modelling has been done using various training functions (RP, CGP and LM), activation functions (LOGSIG and TANSIG) and also optimal number of neurons in the hidden layer. Mean squared errors have been evaluated to estimate the optimized number of neurons in the hidden layer. LM training function with optimal five neurons in hidden layer and TANSIG activation function is found to be the most suitable one for the prediction of CI with an average deviation of 3.11%. Finally, developed mathematical expression has been studied critically to explore the effect of milling parameters on chatter severity. It has been inferred that effects of spindle speed and axial depth of cut on chatter severity is more pronounced as compared to feed rate.

Declarations

References

1. Kim SK, Lee SY (2001) Chatter prediction of end milling in a vertical machining center. J Sound Vib 241:567–586. https://doi.org/10.1006/jsvi.2000.3144

2. Lamraoui M, Thomas M, El Badaoui M (2014) Cyclostationarity approach for monitoring chatter and tool wear in high speed milling. Mech Syst Signal Process 44:177–198. https://doi.org/10.1016/j.ymssp.2013.05.001

3. Peng C, Wang L, Liao TW (2015) A new method for the prediction of chatter stability lobes based on dynamic cutting force simulation model and support vector machine. J Sound Vib 354:118–131. https://doi.org/10.1016/j.jsv.2015.06.011

4. Cao H, Lei Y, He Z (2013) Chatter identification in end milling process using wavelet packets and Hilbert-Huang transform. Int J Mach Tools Manuf 69:11–19. https://doi.org/10.1016/j.ijmachtools.2013.02.007

5. Fu Y, Zhang Y, Zhou H et al (2016) Timely online chatter detection in end milling process. Mech Syst Signal Process 75:668–688. https://doi.org/10.1016/j.ymssp.2016.01.003

6. Ji Y, Wang X, Liu Z et al (2017) EEMD-based online milling chatter detection by fractal dimension and power spectral entropy. Int J Adv Manuf Technol 92:1185–1200. https://doi.org/10.1007/s00170-017-0183-7

7. Delio T, Tlusty J, Smith S (1992) Use of audio signals for chatter detection and control. J Manuf Sci E T ASME 114:146–157. https://doi.org/10.1115/1.2899767

8. Altintas Y, Chan PK (1992) In-process detection and suppression of chatter in milling. Int J Mach Tools Manuf 32:329–347. https://doi.org/10.1016/0890-6955(92)90006-3

9. Schmitz TL, Medicus K, Dutterer B (2002) Exploring once-per-revolution audio signal variance as a chatter indicator. Mach Sci Technol 6:215–233. https://doi.org/10.1081/MST-120005957

10. Quintana G, Ciurana J, Ferrer I, Rodríguez CA (2009) Sound mapping for identification of stability lobe diagrams in milling processes. Int J Mach Tools Manuf 49:203–211. https://doi.org/10.1016/j.ijmachtools.2008.11.008

11. Mishra R, Singh B (2021) Stability analysis in milling process using spline based local mean decomposition (SBLMD) technique and statistical indicators. Meas: J Int Meas Confed 174:108999. https://doi.org/10.1016/j.measurement.2021.108999

12. Ghosh N, Ravi YB, Patra A et al (2007) Estimation of tool wear during CNC milling using neural network-based sensor fusion. Mech Syst Signal Process 21:466–479. https://doi.org/10.1016/j.ymssp.2005.10.010

13. Ritou M, Garnier S, Furet B, Hascoet JY (2014) Angular approach combined to mechanical model for tool breakage detection by eddy current sensors. Mech Syst Signal Process 44:211–220. https://doi.org/10.1016/j.ymssp.2013.02.004

14. Uekita M, Takaya Y (2017) Tool condition monitoring technique for deep-hole drilling of large components based on chatter identification in time–frequency domain. Meas: J Int Meas Confed 103:199–207. https://doi.org/10.1016/j.measurement.2017.02.035

15. Xu X, Zhou T, Hu H, Hu Y (2020) Chatter frequency identification and amplitude tracking using short-time difference spectrum analysis. IEEE Trans Instrum Meas 69:9844–9852. https://doi.org/10.1109/TIM.2020.3003361

16. Lee WK, Ratnam MM, Ahmad ZA (2017) Detection of chipping in ceramic cutting inserts from workpiece profile during turning using fast Fourier transform (FFT) and continuous wavelet transform (CWT). Precis Eng 47:406–423. https://doi.org/10.1016/j.precisioneng.2016.09.014

17. Tran MQ, Liu MK, Tran QV (2020) Milling chatter detection using scalogram and deep convolutional neural network. Int J Adv Manuf Technol 107:1505–1516. https://doi.org/10.1007/s00170-019-04807-7

18. Berger BS, Minis I, Harley J et al (1998) Wavelet based cutting state identification. J Sound Vib 213:813–827. https://doi.org/10.1006/jsvi.1997.1495

19. Yoon MC, Chin DH (2005) Cutting force monitoring in the end-milling operation for chatter detection. Proc Inst Mech Eng Part B: J Eng Manuf 219:455–465. https://doi.org/10.1243/095440505X32292

20. Cai K, Cao W, Aarniovuori L et al (2019) Classification of power quality disturbances using Wigner-Ville distribution and deep convolutional neural networks. IEEE Access 7:119099–119109. https://doi.org/10.1109/ACCESS.2019.2937193

21. Qi K, He Z, Zi Y (2007) Cosine window-based boundary processing method for EMD and its application in rubbing fault diagnosis. Mech Syst Signal Process 21:2750–2760. https://doi.org/10.1016/j.ymssp.2007.04.007

22. Liu C, Zhu L, Ni C (2017) The chatter identification in end milling based on combining EMD and WPD. Int J Adv Manuf Technol 91:3339–3348. https://doi.org/10.1007/s00170-017-0024-8

23. Zhang Q, Tu X, Li F, Hu Y (2020) An effective chatter detection method in milling process using morphological empirical wavelet transform. IEEE Trans Instrum Meas 69:5546–5555. https://doi.org/10.1109/TIM.2019.2958470

24. Zhang Z, Li H, Meng G et al (2016) Chatter detection in milling process based on the energy entropy of VMD and WPD. Int J Mach Tools Manuf 108:106–112. https://doi.org/10.1016/j.ijmachtools.2016.06.002

25. Li Z, Chen J, Zi Y, Pan J (2017) Independence-oriented VMD to identify fault feature for wheel set bearing fault diagnosis of high speed locomotive. Mech Syst Signal Process 85:512–529. https://doi.org/10.1016/j.ymssp.2016.08.042

26. Amezquita-Sanchez JP, Adeli H (2015) A new music-empirical wavelet transform methodology for time-frequency analysis of noisy nonlinear and non-stationary signals. Digit Signal Process: Rev Jl 45:55–68. https://doi.org/10.1016/j.dsp.2015.06.013

27. Pan J, Chen J, Zi Y et al (2016) Mono-component feature extraction for mechanical fault diagnosis using modified empirical wavelet transform via data-driven adaptive Fourier spectrum segment. Mech Syst Signal Process 72–73:160–183. https://doi.org/10.1016/j.ymssp.2015.10.017

28. Smith JS (2005) The local mean decomposition and its application to EEG perception data. J R Soc Interface 2:443–454. https://doi.org/10.1098/rsif.2005.0058

29. Deng L, Zhao R (2014) An improved spline-local mean decomposition and its application to vibration analysis of rotating machinery with rub-impact fault. J Vibroengineering 16:414–433

30. Rangwala S, Dornfeld D (1990) Sensor integration using neural networks for intelligent tool condition monitoring. J Manuf Sci E T ASME 112:219–228. https://doi.org/10.1115/1.2899578

31. Al-Zubaidi S, Ghani JA, Che Haron CH (2011) Application of ANN in milling process: a review. Model Simul Eng. https://doi.org/10.1155/2011/696275

32. Filippis LAC De, Serio LM, Facchini F, Mummolo G (2018) ANN modelling to optimize manufacturing process. In: El-Shahat A (ed) Advanced applications for artificial neural networks. InTech, USA. https://doi.org/10.5772/intechopen.68505

33. Lamraoui M, Barakat M, Thomas M, El BM (2015) Chatter detection in milling machines by neural network classification and feature selection. JVC/J Vib Control 21:1251–1266

34. Kumar S, Singh B (2019) Ascertaining of chatter stability using wavelet denoising and artificial neural network. Proc Inst Mech Eng C J Mech Eng Sci 233:39–62. https://doi.org/10.1177/0954406218756440

35. Zhu W, Zhuang J, Guo B et al (2020) An optimized convolutional neural network for chatter detection in the milling of thin-walled parts. Int J Adv Manuf Technol 106:3881–3895. https://doi.org/10.1007/s00170-019-04899-1

36. Sheela KG, Deepa SN (2013) Review on methods to fix number of hidden neurons in neural networks. Math Probl Eng. https://doi.org/10.1155/2013/425740

37. Altintaş Y, Budak E (1995) Analytical prediction of stability lobes in milling. CIRP Ann Manuf Technol 44:357–362. https://doi.org/10.1016/S0007-8506(07)62342-7